Electronic Supplementary Information (ESI) for

Structural characterization of supramolecular hollow nanotubes with atomistic simulations and SAXS

Ilias Patmanidis,[a] Alex H. de Vries,[a] Tsjerk A. Wassenaar,[a] Wenjun Wang,[b] Giuseppe Portale,[c] Siewert J. Marrink*[a]

[a] *Groningen Biomolecular Science and Biotechnology Institute and Zernike Institute for Advanced Materials, University of Groningen, Groningen, the Netherlands.*
[b] *Leiden University Medical Center, Leiden, The Netherlands.*
[c] *Department of Polymer Chemistry, Zernike Institute for Advanced Materials, University of Groningen, Groningen, The Netherlands.*

E-mail: s.j.marrink@rug.nl

1 C8S3 parametrization

QM calculations were employed to optimize the description of the aromatic core of the C8S3 molecule. Specifically, we focused on the dihedral potentials of the polymethine bridge and the partial charges of the monomer. To reduce the size and complexity of the system and concentrate on the native conformations and dynamics of the core, we prepared the C1C1 molecule (see Figure S1A), that shares the same aromatic backbone as C8S3, and used it as a reference for our calculations. Smaller systems tend to be more accurate and less expensive for calculations at the QM level.

The description for the dihedrals of the linker between the two aromatic rings was examined by performing potential energy scans of the C5-C3-C2-C4 and N9-C5-C3-C2 dihedrals by rotating in steps of 10° around the torsional angles and measuring the energy in each conformation (see Figure S1A). At each value of the dihedral angle of interest, all other degrees of freedom were fully relaxed during the minimization procedure. The dihedral profiles for torsions around the bonds C5-C3-C2-C4 and N9-C5-C3-C2, respectively, are presented in Figure S1B and the force constants for the fitted dihedrals in Table S1. The phase and the multiplicity of all torsional angles was 180° and 2, respectively.

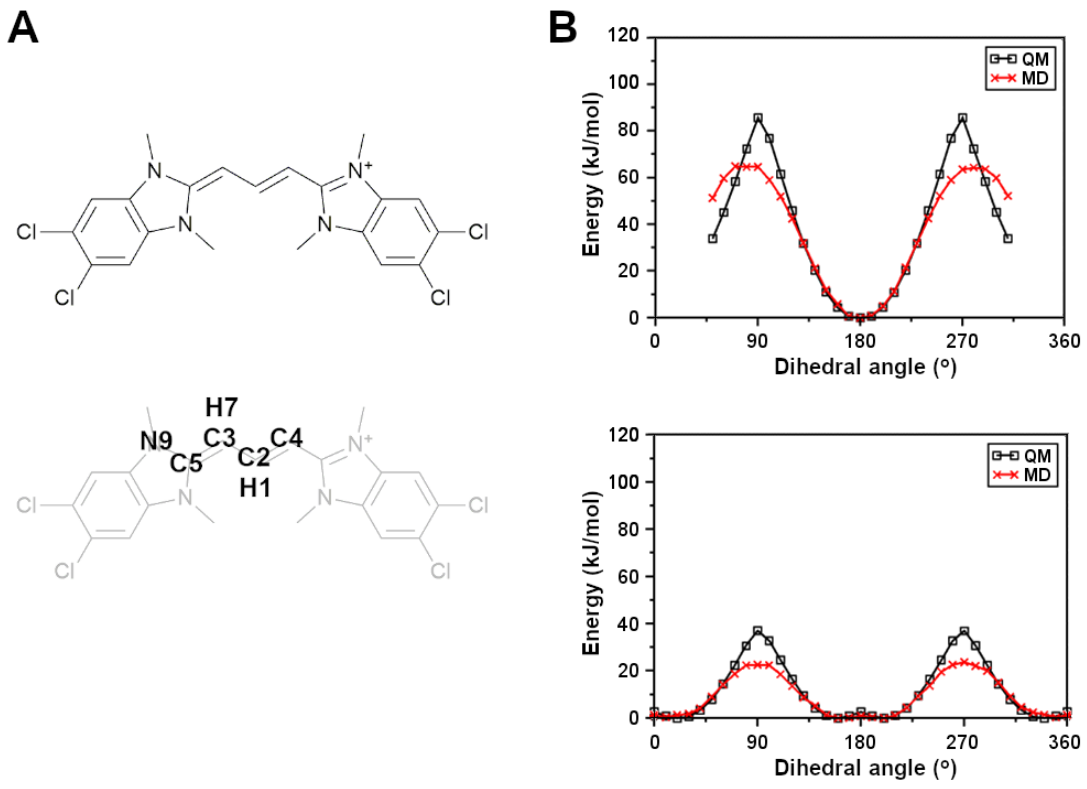

Figure S1: Force field optimization using QM. (A) Chemical structure of C1C1 monomer. The atoms involved in the dihedral angle definitions are highlighted on the bottom panel. (B) Potential energy profiles for dihedrals C5-C3-C2-C4 (top) and N9-C5-C3-C2 (bottom). The QM curve represents the energy profile calculated from the QM calculation, and the MD profile represents the final energy profile after including the calculated dihedral parameters.

Table S1: Dihedral definitions for the atoms of the polymethine bridge.

Dihedral	Force constant (kJ/mol)
H1-C2-C3-H7	6.44
C5-C2-C3-C4	25.74
N9-C5-C3-C2	19.30
N9-C5-C3-H7	4.82

The MD profiles were in good agreement with the QM profile. We were able to reproduce the width of the well near the energy minimum. The reason for not being able to capture the height of the curves is the type of dihedrals that we decided to use for these descriptions. Modelling the dihedral potentials with more complex descriptions rather than simple cosine functions could give better agreement with the QM energy profiles, but was beyond the scope of this study. The systems in the QM calculations became unstable for dihedral angles lower than 50° and higher than 310° due to steric clashes, so this part of the energy profile could not be calculated and is excluded from the plot.

Additionally, the partial charges of C1C1 and C8S3 have been calculated at QM level. The partial charges of C1C1 and C8S3 were calculated at the optimum geometry, and the raw values resulting from the DPA analysis[1] were rounded to the second decimal to maintain symmetry and simplicity. Some values were adapted to maintain integer net charges. We assume that the distribution of the partial charges would be more accurate for the less complex system, so C8S3 charges were rounded according to the C1C1 charges. The partial charge of the atoms belonging to the aliphatic tails was set to 0 in accord with standard G53a6[2] charges for united-atom aliphatic chains. Partial charges for each atom of C1C1 and C8S3 are reported in Table S2.

Table S2: QM and final MD partial charges for C1C1 and C8S3

Atom	QM C1C1	Final C1C1	C8S3	Final C8S3
H1	0.0476	0.03	0.0007	0.02
C2	-0.0442	-0.03	-0.0265	-0.02
C3	-0.2366	-0.25	-0.292	-0.27
C4	-0.2694	-0.25	-0.2548	-0.27
C5	0.6774	0.66	0.6788	0.67
C6	0.6675	0.66	0.6545	0.67
H7	0.0244	0.03	0.0586	0.06
H8	0.0459	0.03	0.0611	0.06
N9	-0.3486	-0.39	-0.3785	-0.39
N10	-0.3406	-0.39	-0.381	-0.39
N11	-0.3786	-0.39	-0.4205	-0.39
N12	-0.3614	-0.39	-0.4236	-0.39
C13	0.282	0.28	0.3152	0.3
C14	0.2937	0.28	0.3378	0.3
C15	0.2799	0.28	0.3125	0.3
C16	0.2828	0.28	0.2895	0.3
C17	-0.1822	-0.16	-0.2054	-0.2
C18	-0.1893	-0.16	-0.2321	-0.2
C19	-0.1893	-0.16	-0.2321	-0.2
C20	-0.1991	-0.16	-0.2118	-0.2
C21	0.002	0.02	0.0198	0.02
C22	0.0338	0.02	0.0135	0.02
C23	0.0765	0.02	0.0263	0.02
C24	0.0346	0.02	0.027	0.02
H25	0.0971	0.11	0.133	0.13
H26	0.1006	0.11	0.1592	0.13
H27	0.0797	0.11	0.1135	0.13
H28	0.1067	0.11	0.0977	0.13
CL29	-0.0323	-0.03	-0.0805	-0.09
CL30	-0.0347	-0.03	-0.1019	-0.09
CL31	-0.0343	-0.03	-0.0792	-0.09
CL32	-0.0346	-0.03	-0.0913	-0.09
H/C33	0.2016	0.2	0.1314	0.16
H/C34	0.192	0.2	0.1141	0.16
C35	-	-	0.0844	0.0
C36	-	-	0.0946	0.0
C37	-	-	-0.1451	-0.12
C38	-	-	-0.1505	-0.12
S39	-	-	1.1588	1.16
S40	-	-	1.1583	1.16
O41	-	-	-0.6065	-0.62
O42	-	-	-0.6602	-0.62
O43	-	-	-0.6054	-0.62
O44	-	-	-0.6061	-0.62
O45	-	-	-0.6611	-0.62
O46	-	-	-0.6035	-0.62
H/C47	0.176	0.2	0.1262	0.16
H/C48	0.183	0.2	0.1957	0.16
C49	-	-	0.034	0.0
C50	-	-	0.009	0.0
C51	-	-	-0.0065	0.0
C52	-	-	0.0079	0.0
C53	-	-	0.0166	0.0
C54	-	-	0.0006	0.0
C55	-	-	-0.0009	0.0
C56	-	-	0.006	0.0
C57	-	-	0.0069	0.0
C58	-	-	0.0117	0.0
C59	-	-	0.0414	0.0
C60	-	-	0.044	0.0
C61	-	-	-0.0442	0.0
C62	-	-	-0.0422	0.0

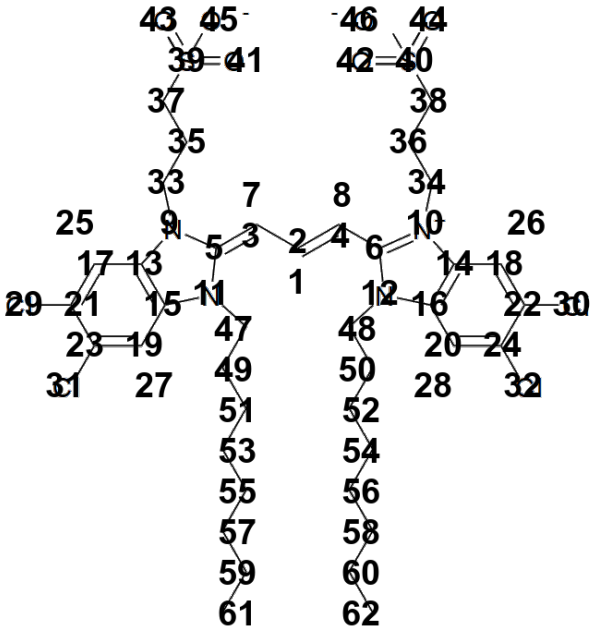

Atom order of C8S3 molecule.

2 C8S3 bilayers

Several systems in which C8S3 molecules were arranged in lamellar formations were prepared. Different setups were used to study the effect of the choice of force field, the initial arrangement and other simulation parameters. A list of all the simulated systems is presented in Table S3.

Table S3: Summary of simulated C8S3 bilayer systems.

	Force field	Formation	Initial box size (nm)	No. C8S3	No. water	No. MeOH	Temperature (K)	Simulation time (ns)
System 1	G53a6	Brickwork	10.69x7.05x10.00	200	15491	-	300	500
System 2	G53a6	Herringbone	8.78x7.72x10.00	198	13354	-	300	500
System 3	G53a6	Staircase	10.85x8.75x10.00	198	19437	-	300	500
System 4	G53a6	Brickwork	10.69x7.05x10.00	200	15491	-	288	250
System 5	G53a6	Herringbone	8.78x7.72x10.00	198	13354	-	288	250
System 6	G53a6	Staircase	10.85x8.75x10.00	198	19437	-	288	250
System 7	G53a6	Brickwork	11.33x7.47x8.27	200	10835	1738	300	250
System 8	G53a6	Herringbone	9.5x8.5x7.95	198	9152	1498	300	250
System 9	G53a6	Staircase	10.39x8.38x9.33	198	13080	2180	300	250
System 10	GAFF	Brickwork	10.69x7.05x10.00	200	14624	-	300	250
System 11	GAFF	Herringbone	8.78x7.72x10.00	198	12825	-	300	250
System 12	GAFF	Staircase	10.85x8.75x10.00	198	18611	-	300	250

In order to avoid potential artifacts caused by the method of measuring the bilayer thickness, different approaches were used (see Table S4). The bilayer thickness was calculated by monitoring the distance between the center of mass of the SO_3^- groups in each leaflet, a typical measure to calculate the thickness of lipid bilayers based on the position of the PO_4^- group. Electrons density profiles across the bilayer were generated and the distance between the highest peak of each leaflet was measured as an alternative measure of the thickness, which is in principle accessible through electron scattering. We keep in mind that the center of mass distance and electron density calculations could be affected by undulations of bilayers and can produce unrealistic results when these undulations are large. To avoid overestimation of the bilayer dimensions, we also measured the thickness of small leaflet patches ($\sim$10 nm^2) by monitoring the distance between oxygens of the hydrophilic tails. We found that the method of calculating the bilayer thickness does not dramatically change the measurements, which are always smaller than 3 nm.

Apart from the thickness, additional structural properties of the C8S3 bilayers were monitored to quantify the organization of the C8S3 monomers in the lamellar formations (see Table S5). The orientation of the alkyl tails was measured by calculating the average P_2 order parameter (described in the main article) for the angle between the bilayer normal and the vectors defined by each C-C bond. For the area per molecule, the size of the box in the x- and y-axis was monitored and divided by the number of C8S3 molecules in each leaflet. Last, the diffusion of the monomers was computed by calculating the mean square displacement of the SO_3^- in the plane perpendicular to the z-axis. Standard errors are reported for each measurement.

Table S4: Comparison of the C8S3 bilayer thickness measured with different approaches.

	COM distance (nm)	Electron density distance (nm)	Average distance of small small patches (nm)
System 1	2.41±0.01	2.35±0.01	2.29±0.01
System 2	2.59±0.01	2.88±0.01	2.50±0.01
System 3	2.34±0.01	2.50±0.01	2.25±0.02
System 4	2.40±0.01	2.42±0.01	2.29±0.01
System 5	2.55±0.01	2.81±0.01	2.57±0.03
System 6	2.36±0.01	2.33±0.01	1.86±0.01
System 7	2.45±0.01	2.37±0.01	2.36±0.02
System 8	2.55±0.01	2.80±0.01	2.21±0.06
System 9	2.34±0.01	2.46±0.01	2.27±0.03
System 10	2.59±0.01	2.58±0.01	2.45±0.01
System 11	2.76±0.01	2.72±0.01	2.76±0.35
System 12	2.52±0.01	2.55±0.01	2.38±0.04

Table S5: Bilayer properties in different simulations.

	Tail order parameter	Area per molecule [a] (nm^2)	Diffusion ($\mu m^2/s$)
System 1	0.20±0.01	0.890	3.2±1.0
System 2	0.15±0.01	0.802	6.2±6.6
System 3	0.11±0.01	0.886	6.4±2.4
System 4	0.21±0.01	0.900	5.9±0.2
System 5	0.14±0.01	0.814	8.4±3.3
System 6	0.10±0.01	0.881	7.8±1.9
System 7	0.19±0.01	0.898	8.2±5.8
System 8	0.19±0.01	0.898	8.2±5.8
System 9	0.14±0.01	0.829	8.3±3.6
System 10	0.11±0.01	0.889	10.4±3.7
System 11	0.31±0.01	0.868	3.6±2.7
System 12	0.30±0.01	0.818	6.2±1.3

[a] Errors: $<< 0.001$

Statistical analyses for different observables as a function of time are presented in Figure S2. We consider the bilayer simulations as an exploratory study to obtain a reasonable initial thickness for the nanotube simulations. Even if the sampling of certain observables in individual simulations might not be enough (the area and thickness of the SC has a drift), the simulation length should be adequate for a preliminary study.

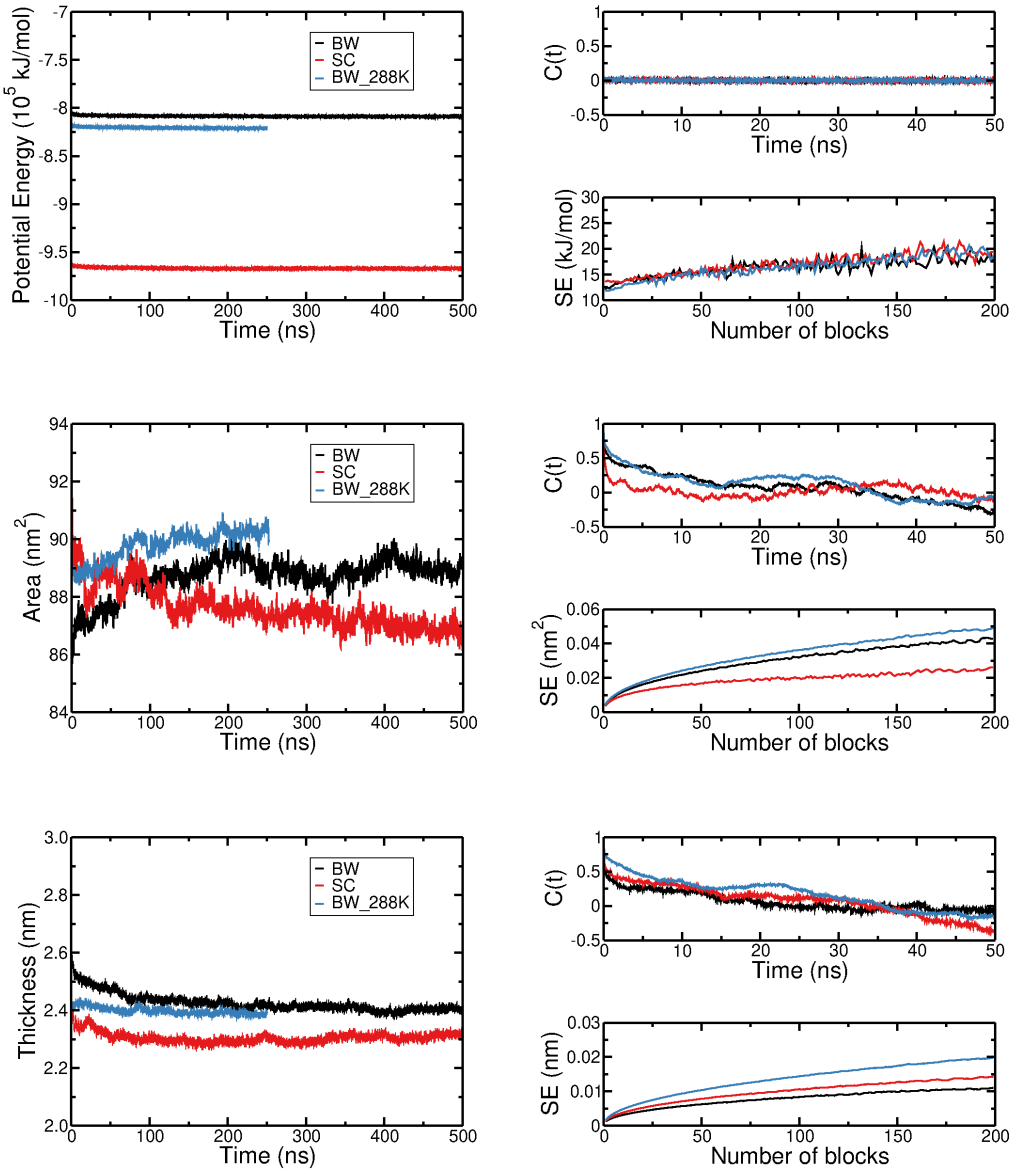

Figure S2: Observables from simulations as a function of time: a) potential energy, b) bilayer area, and c) bilayer thickness. BW: System 1 with Brickwork formation at 300 K, SC: System 3 with Staircase formation at 300 K and BW_288K: System 4 with Brickwork formation at 288 K. The autocorrelation and standard errors for each measurement are reported on the right of each panel. The statistical analysis was performed for the last 100 ns of the bilayers.

The similarity of the simulated structures with respect to the initial conformation was compared by plotting the Radial Distribution Function (RDF) and P_2 parameter of different groups of atoms and is shown in Figure S3.

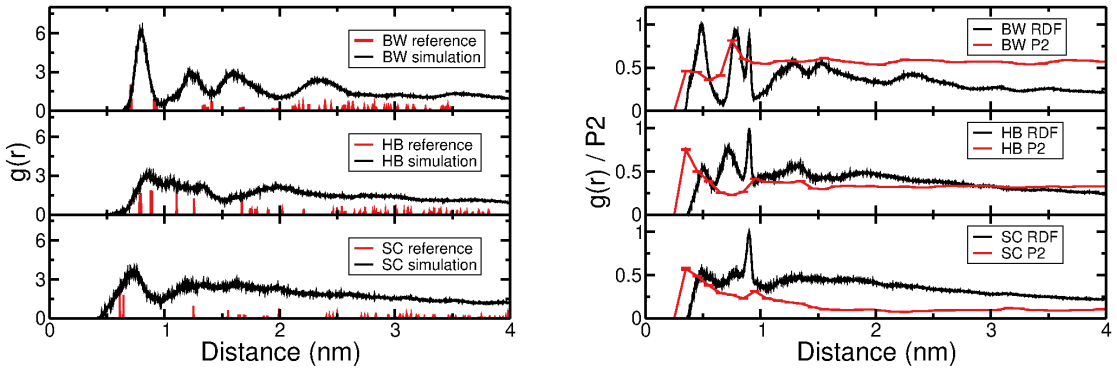

Figure S3: RDF and P2 order parameter for the longest bilayer simulations with the Brickwork (BW), Herringbone (HB) and Staircase (SC) formations. The RDF of the reference structure for the central atom of the aromatic core (C2) is superimposed with the RDF during the last 100 ns each simulation (left). RDF and P2 order parameter for the center and the plane of the benzimidazole ring (right). The small error bars for P2 indicate that the arrangements hardly change during the simulations Both figures show that the degree of order is higher in the BW formation, lower in the HB and completely lost in the SC formation, in which the aromatic rings are randomly oriented beyond 1 nm.

3 C8S3 nanotubes

Short and long C8S3 nanotubes were constructed with different initial arrangements and dimensions. The procedure is described in the main article and the parameters used are reported in Table S6. Specifically, the distance of the SO_3^-/polymethine bridge (PMB) from the center of the tube is reported. The construction of the nanotubes was based on the radius of the polymethine bridge, which coincides with the radius of the chromophore. The rolling angle for each wall, simulation time and nanotube length are also reported. The thickness of the nanotubes at the beginning of the simulations was ∼3 nm, since the C8S3 monomers were flat and stretched to avoid atom overlaps in the initial conformation. Effectively, the thickness would be ∼2.5 nm, when the tails adopt a more natural configuration. The system with a star (*) was performed with the GAFF force field.

The dimensions of the C8S3 nanotubes at the end of the simulations are reported in Table S7. The thickness was calculated by measuring the average distance of the inner and outer SO_3^- groups from the center of the nanotube and taking their difference.

Statistical analysis for the measured thickness as a function of time is presented in Figure S4. The bump during the 10 ns is caused due to the removal of the position restraints that were keeping the aromatic cores of the C8S3 molecules fixed.

Table S6: Initial parameters for the preparation of C8S3 nanotubes simulations.

System	No. C8S3	Inner radius SO_3^-/PMB (nm)	Inner rolling angle (°)	Outer radius SO_3^-/PMB (nm)	Outer rolling angle (°)	Simulation time (ns)	Length (nm)
Herringbone 1	1319	3.33/4.00	31.35	6.43/5.73	31.37	100	15
Herringbone 2	1515	4.02/4.73	31.29	7.17/6.46	31.08	100	15
Brickwork 1	1289	3.31/4.00	31.35	6.43/5.73	31.37	100	15
Brickwork 2	1098	2.58/3.27	32.40	5.71/5.00	31.75	100	15
Herringbone Long 1	8275	3.03/3.73	31.17	6.42/5.72	21.60	10	100
Herringbone Long 1*	8275	3.03/3.73	31.17	6.42/5.72	21.60	10	100

Table S7: Final dimensions of C8S3 nanotubes simulations.

System	Inner radius (nm)	Outer radius (nm)	Thickness (nm)
Herringbone 1	4.09 ± 0.51	6.40 ± 0.40	2.31 ± 0.03
Herringbone 2	4.73 ± 0.47	7.12 ± 0.34	2.39 ± 0.03
Brickwork 1	4.55 ± 0.39	6.93 ± 0.36	2.37 ± 0.04
Brickwork 2	3.86 ± 0.49	6.18 ± 0.37	2.31 ± 0.04
Herringbone Long 1	3.71 ± 0.07	6.19 ± 0.06	2.48 ± 0.04
Herringbone Long 1*	3.68 ± 0.05	6.31 ± 0.07	2.63 ± 0.05

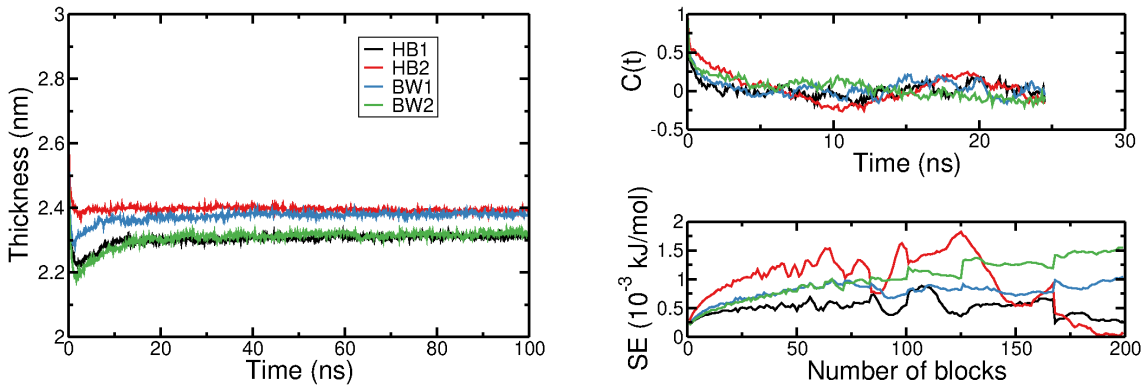

Figure S4: Nanotube thickness as a function of time. The autocorrelation and standard errors for each measurement are reported on the right of each panel. The statistical analysis was performed for the last 50 ns of the short bilayer simulations.

In order to show that the water was properly equilibrated during the simulations inside and outside of the C8S3 nanotubes, the water density at different stages of the system preparation and at the end of the production phase is shown in Figure S5.

The initial and the final arrangement for different simulations is shown in Figure S6.

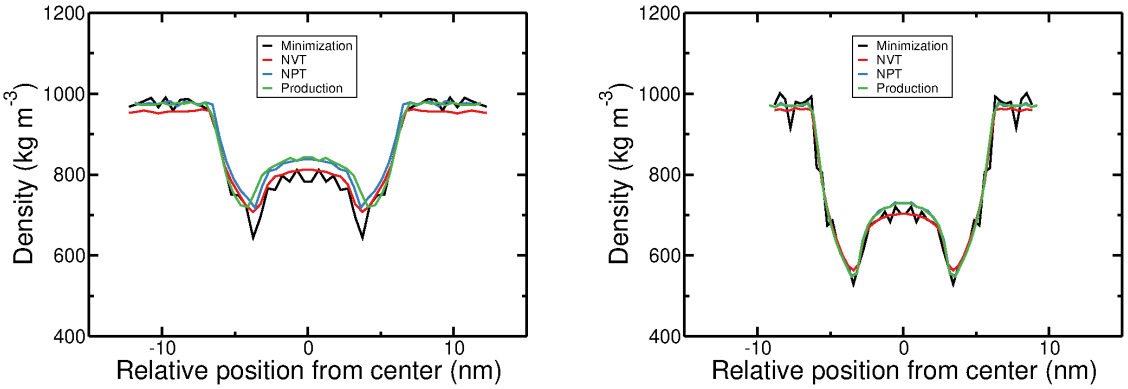

Figure S5: Water density of simulation boxes along the x-axis at different time frames, a short nanotube (left) and a long nanotube (right). At the end of the minimization and NVT equilibration steps, the water molecules inside the tubes are depleted, mainly due to the stretched tails of the monomers (to avoid atom overlaps between C8S3) that contract in the beginning of the simulation. During the longer NPT equilibration steps, the tails are relaxed and the water inside and outside of the box is equilibrated.

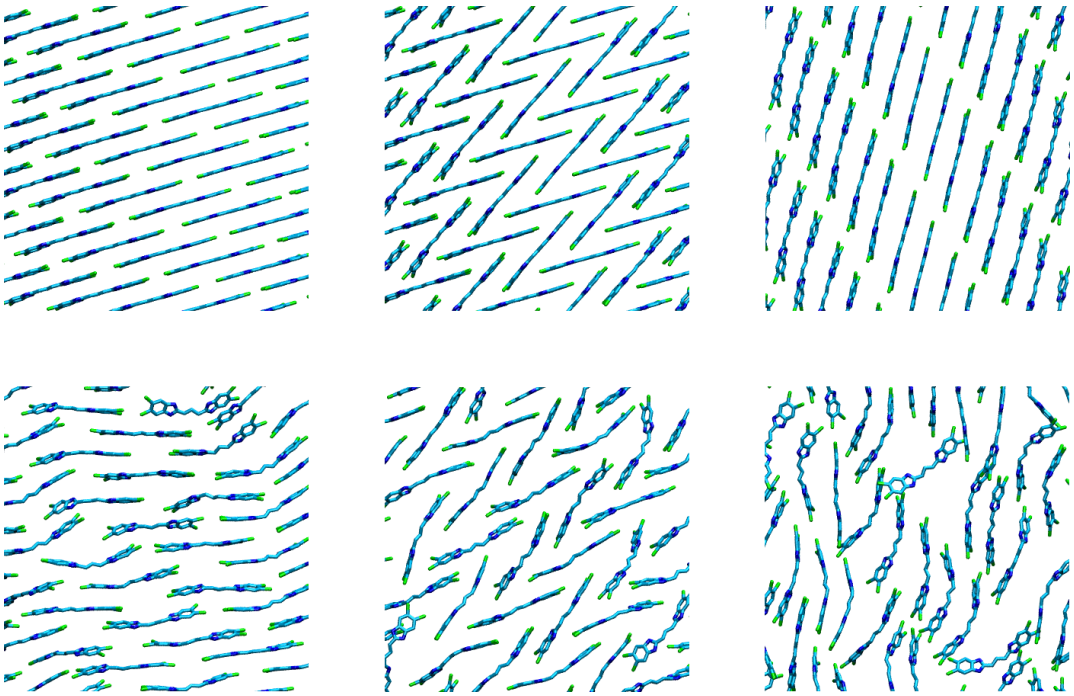

Figure S6: Snapshots of the C8S3 arrangement in nanotubes at the beginning and the end of simulations: brickwork (left), herringbone (middle) and staircase arrangement (right). The snapshot was taken at 100 ns for the brickwork and herringbone formation and at 10 ns for the staircase formation. The side chains are not shown for clarity.

The short C8S3 nanotube simulations were used to obtain MD simulated spectra[3] that were compared to the experimental SAXS results. The superimposition of all simulated and experimental spectra are presented in Figure S7. The agreement is quite remarkable, especially for Herringbone 1 and Brickwork 2 systems, indicating that their dimensions are most likely closer to the real values. The same trends can also be observed in the superimposition of the electron density profiles from the short C8S3 nanotube simulations with the contrast profile from cryo-TEM experiments[4] (see Figure S8).

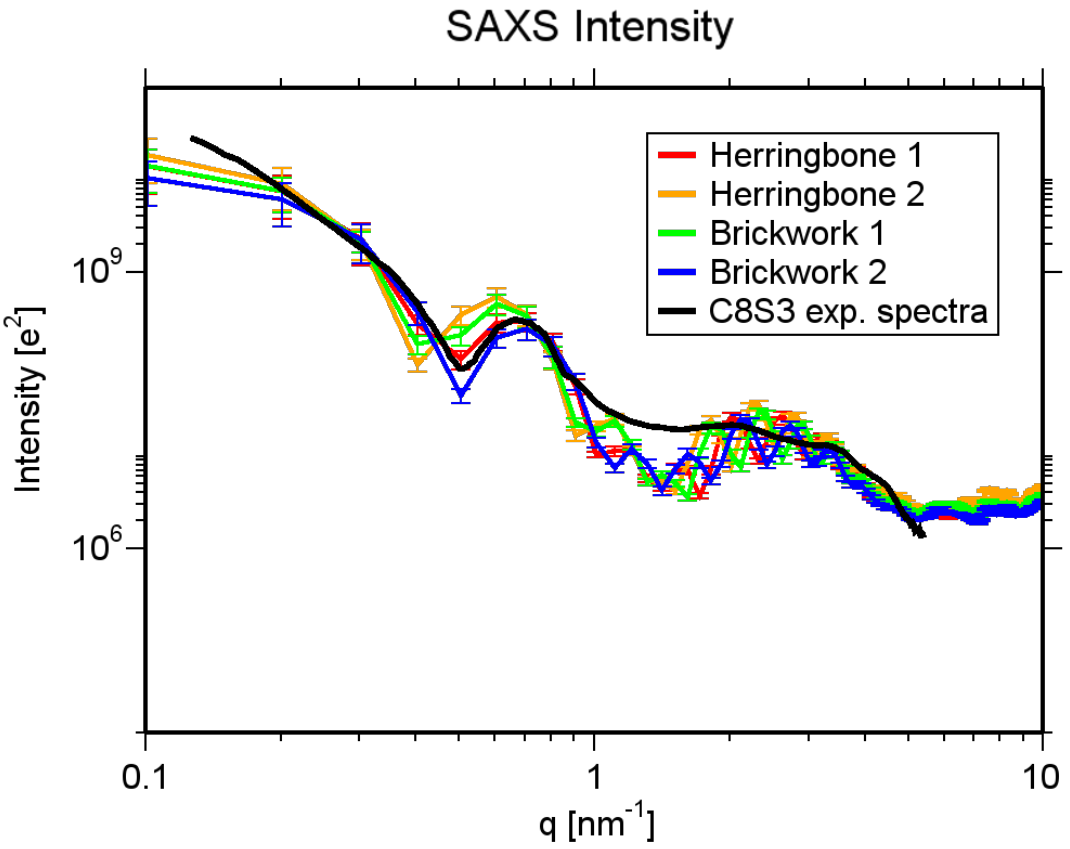

Figure S7: Comparison of SAXS spectra and MD simulated spectra from short C8S3 nanotube simulations.

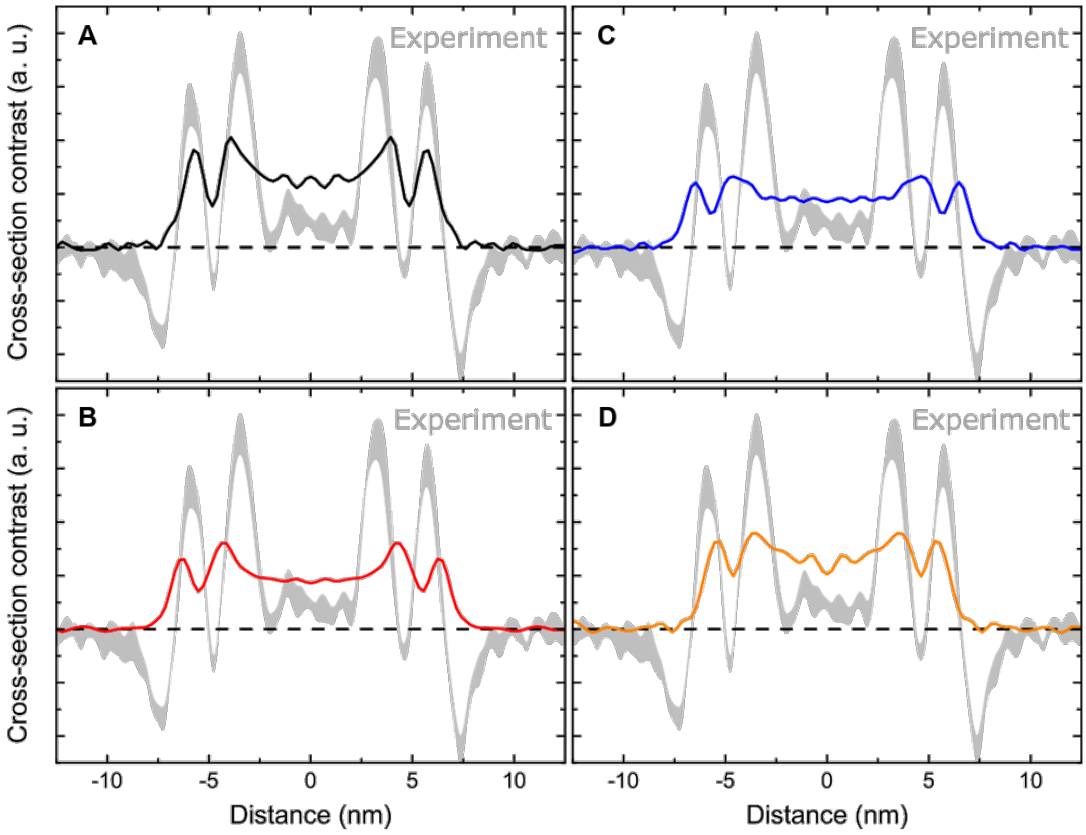

Figure S8: Comparison of a cryo-TEM cross-section and the projected electron density from short C8S3 nanotube simulations, (A) Herringbone 1, (B) Herringbone 2, (C) Brickwork 1 and (D) Brickwork 2.

Last, snapshots from a deformed C8S3 nanotube are shown in Figure S9. The nanotube was designed to be continuous along the periodic boundary conditions of the simulation box.

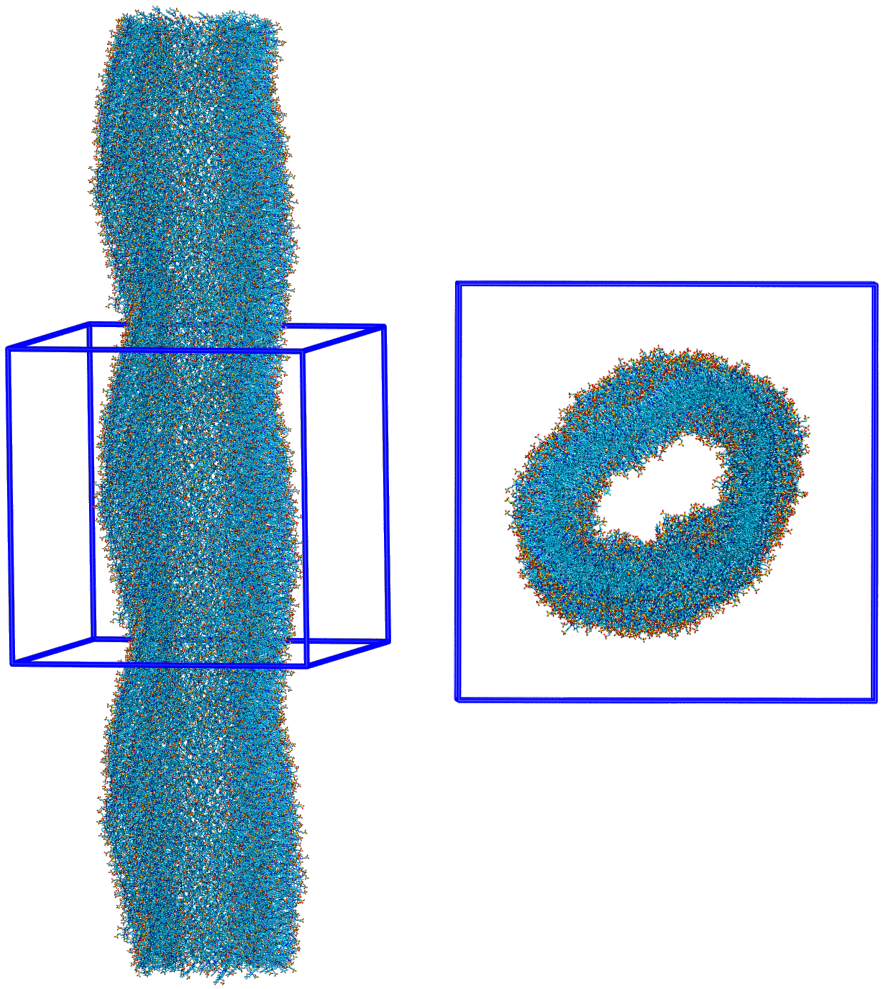

Figure S9: Snapshots from the periodic C8S3 nanotube after 10 ns of simulation, side view (left) and top view (right).

References

[1] B. T. Thole and P. T. van Duijnen, *Theoretical Chemistry Accounts*, 1983, **63**, 209–221.

[2] C. Oostenbrink, A. Villa, A. E. Mark and W. F. Van Gunsteren, *Journal of Computational Chemistry*, 2004, **25**, 1656–1676.

[3] P. Chen and J. Hub, *Biophysical Journal*, 2014, **107**, 435–447.

[4] B. Kriete, J. Lüttig, T. Kunsel, P. Malý, T. L. C. Jansen, J. Knoester, T. Brixner and M. S. Pshenichnikov, *Nature Communications*, 2019, **4615**,.